International Journal of mining and Geo-Engineering

IJMGE

IJMGE 51-2 (2017) 199-207

DOI: 10.22059/ijmge.2017.212587.594618

Faults and fractures detection in 2D seismic data based on principal component analysis

Poorandokht Soltani [a], Mehrdad Soleimani [a], Hamid Aghajani [a, *]

[a] *Faculty of Mining, Petroleum & Geophysics Engineering, Shahrood University of Technology, Shahrood, Iran*

Article History:

Received: 31 July 2016,
Revised: 26 August 2017,
Accepted: 13 September 2017.

ABSTRACT

Various approached have been introduced to extract as much as information from seismic images for any specific reservoir or geological study. Faults and fractures modeling is among the most attracted objectives of geological studies on seismic images. Several strategies have been presented for this specific purpose. In this study, we have presented a modified approach of application concept of the principle components analysis to enhance faults and fractures from low quality seismic images. In the first step, relevant attributes considering imaging faults and fractures were drawn based on extensive studies on previous successful applications of different attributes. Subsequently, major informative components of each attribute were defined by performing principle component analysis. Since random noise in seismic images exhibits no correlation in seismic data, true reflectors and diffraction events show a high coherency value; thus, these objects are separated into different orthogonal components in principle component analysis. It makes it easy to remove irrelevant information considering faults and fractures from a seismic image, and thus, combining the attribute sections in principle component analysis produce a higher quality image. Afterwards, the selected components were stacked to enhance the fault position in final image. However, since there were other geological objects that might show a correlation with other orthogonal components, the refinement step should be applied on the final image to stack only the desired information. This approach was performed on a field land data example form northeast of Iran. Results of the proposed strategy show that this method is capable to image faults compared to conventional image analysis for fault detection. The method is also capable to image the accurate position of the body of mud volcanoes extracted from the image that could not be easily tracked by conventional seismic image analysis.

Keywords : *Attributes, Faults and fracture, Mud volcano, Principle component analysis, Seismic*

1. Introduction

Seismic sections show an image of geological objects from subsurface containing layer boundaries, faults, and structural features. However, seismic data also exhibits some not geologically related information such as random or coherent noise and reflection from outside of the profile. According to the aim of seismic study, different geological object from seismic data should be enhanced and geologically interpreted. Faults are among the most important geological events that have attracted much attention in subsurface geological studies. Accurate imaging of faults and fractures plays an important role in many geological studies such as drilling path identification, petroleum reservoir exploration and gas injection studies. In petroleum exploration drilling, faults should be identified preciously before designing drilling path and have to be avoided during drilling. In seismic reservoir studies, fractures show the zone of high productivity and faults show the top of the reservoir whether it is a sealed or a leaking zone. Leaking faults might also create a gas chimney in petroleum or gas reservoirs with gas cap, which is an identification of petroleum reservoir exploration. Accordingly, accurate interpretation of faults and fractures in seismic imaging (SI) is required for reservoir characterization studies, as well as static and dynamic reservoir modeling.

There are various methods to automatically, or semi-automatically, image faults and fractures from seismic images. Principal component analysis (PCA) is a mathematical analytical approach that extracts the relevant information from any datasets based on the objectives of the study. The PCA analysis has found its major use in geoscience and in remote sensing (RS) image analysis. After successful application of PCA in RS and its fast development in RS image analysis, PCA was extended to be used in other geoscience studies such as SI analysis. Since the source of data, both in RS and SI, are in type of images, thus, same strategies could be used for same aim of studies. For example, fault and fracture analysis in SI could be used by approaches that conventionally have been applied on RS [1]. Due to the nature of seismic images, they contain variety of information of subsurface layers and structures in the form of wave propagation equations that cannot be illustrated in a single image and have to be extracted by any means from seismic data. Seismic attribute analysis is an interpretation tool that provides the related information of wave propagation equation in subsurface, and is used for any geological modeling. Seismic attribute analysis is widely used for any specific geological interpretation from 2D and 3D seismic data. Some attributes are designed for structural interpretation while some other are used only for stratigraphical studies. In addition, seismic attributes can be used for other various types of geological studies such as salt dome detection, gas chimney identification, gas hydrate exploration and fault and fracture analysis [2]. Since seismic attributes provides a large amount of seismic images, which show a specific character of the seismic images related to any properties of subsurface structures, thus, the PCA method can be used to classify the required information and remove unwanted images in seismic attribute analysis. Therefore, the PCA analysis is used to obtain the most related seismic

* Corresponding author. *E-mail address:* aghajani_hamid@yahoo.com (H. Aghajani).

attributes according the objectives of the study, among the large number of related and unrelated attributes [3]. Based on geological characteristics of the target, several approaches in PCA can be used for attribute analysis. The PCA method was successfully applied on orthogonal decomposition of seismic surfaces (maps) for fault detection [4]. The PCA analysis was also used on 3D seismic attributes for petroleum reservoir characterization and for fault and fracture detection in other geophysical images such as geo-electric images [5], [6]. However, due to the large size of seismic data, fault and fracture detection in seismic images should be performed automatically with high accuracy. Therefore, various techniques with specific engine search and selection criteria were introduced for automatic fault detection [7]. Generalized earthmovers distance as a searching engine and classifier was used for automatic fault detection in seismic data [8]. In some cases, this automatic fault detection approach can interact with interpreter and should perform on graphical hardware for large seismic data. In this study, we introduce a PCA approach for semi-automatic fault detection on seismic attributes combined with RGB filters used in RS image analysis. The attributes were selected based on previous successful application of related attributes used for fault detection from seismic images. This approach was applied on a field example from northeast of Iran, containing mud volcanoes, fault zone and an unconformity that separate these two objects. Since the proposed approach is capable to identify truncations in seismic reflector known as layers, it can preciously image the boundary of mud volcanoes with other sediment layers, as well.

2. Methodology

Geological model building and identification of geological objects in seismic data is somehow difficult due to distortions that happens to seismic images through wave propagation in subsurface and seismic data processing steps to the final images. However, faults and fractures are known in seismic sections as a trend in truncation of reflectors or layers. Generally, faults produce diffractions that are used through seismic data processing to image the faults in the final seismic image [9]. The first step in presenting the proposed approach in this study is to perform an attribute analysis step. Seismic attributes exhibit physical properties of wave propagating in the media containing the geological and the media information such as acoustic impedance contrast between layers, reflection coefficient of layer boundaries, seismic velocity and energy absorption of layers [10]. Thus, it is necessary to select the most relevant attribute and/or physical parameter that can be used to enhance fault and fractures in seismic images, and suppress other unwanted objects. This was performed by a survey on numerous published successful applications of attributes on fault analysis shown in Table 1. As Table 1 shows, usually chaos, first and second derivatives, variance, maximum and minimum curvatures and the most positive and negative curvatures are used as the main attributes for fault enhancement. Application of a single attribute might reveal an accepted level of information required for imaging specific fault in a seismic image, but it would be an advantage if we combine different relevant attributes to enhance more faults in a seismic image.

Table 1. Attributes used for fault enhancement and geological boundary detection.

Attribute	Application	Study
Chaos	Salt dome, river channel and mud volcano detection.	[11], [12]
First derivative	Unconformity, fault enhancement geological boundary detection,	[13], [14], [15]
Second derivative	Unconformity, fault enhancement geological boundary detection,	[16], [17]
Variance	Salt dome, channel and mud volcano, fault enhancement.	[11], [18]
Most minimum curvatures	Unconformity, fault enhancement geological boundary detection,	[19], [20]
Most maximum curvatures	Unconformity, fault enhancement geological boundary detection,	[21], [22], [23]
Most positive curvatures	Salt dome, channel and mud volcano, Unconformity, fault enhancement,	[24], [25]
Most negative curvatures	Salt dome, channel and mud volcano Unconformity, fault enhancement	[13], [26], [27]

Combination of attributes also results in reduction of coherent and non-coherent noise; increasing quality of the final image and removing artifacts that might exists in the attribute section [14]. Therefore, various studies have been performed in combination of seismic attributes for any specific study. Most of these methods use Artificial Intelligence (AI), Artificial Neural Network (ANN), fuzzy logic, geo-statistical approaches, supervised and unsupervised clustering and PCA methods. The last method uses a converting function in the vector space of data and applies an orthogonal linear transform on them. This orthogonal transformation will transfer data to a new coordinate system from their previous position. The new coordinate system in PCA is designed based on distribution of data in different directions of coordinate space. To apply this transformation in PCA, it is required to perform some statistical analysis in the beginning, which starts with calculating variance of data in different directions. Afterwards, the new coordinate system is designed in a way that the first axis coincides with the direction of the largest value of calculated variance. Subsequently, the second axis coincides with the next largest variance value and it continues for other direction of the new coordinate system. Finally, the last axis is in the direction of the smallest value of the variance in data. Thus, the size of the dataset would be reduced according to the number of axes. The percentage of information in axes of new coordinate system, gives an idea of weighting for further combination of information related to any axis. Rationally, larger weights are allocated to the axis containing more information (called major axes or principal components) and less informative axes (called minor axes) are removed from the combining process through allocation of zero weights to them. Now, if one considers each axis as an attribute section, thus the PCA method makes new attribute by any arbitrary combination of desired attributes, which can be useful for any specific interpretation process. These new attributes are made by combination of major axes (principal components) that do not show any internal relationship and are linearly uncorrelated. In order to define the desired combination of these components, Eigen values and Eigenvectors of the covariance matrix of data should be calculated to define the number of linearly independent attributes. Subsequently, eigenvalues are descending sorted and the highest eigenvalue shows the first main components of the dataset (PC1). The first main component represents the vector with highest variance in data and contains the highest percentage of information that can be used in deriving new attributes. Similarly, the second special vector with the second highest Eigenvalue is called the basic second component (PC2); it depicts a lower variance and is orthogonal to PC1. Likewise, the third principal component (PC3) is orthogonal to the two previous components and so on. After defining the principal components of the data, it is required to decide which attributes should be allocated to each component. In other words, it should be defined that which attributes contain the highest information regarding imaging the faults in seismic data [28]. Various studies have shown that seismic attributes such as dip, azimuth, and coherence were successfully used to define the orientation of faults in seismic data [13]. These attributes were common in showing higher values in faults position of seismic section and exhibit low values in other parts. According to Table 1 that shows application of various attributes in detection of faults, chaos, variance, most positive curvature, most negative curvature, minimum curvature, maximum curvature, the first and second derivatives were selected for this study. PCA for structural interpretation of seismic data expands reflections into orthogonal components, based on computation of eigenvalues and eigenvectors of two-dimensional autocorrelation function. The main idea of the proposed strategy for application of PCA for seismic data is to consider the seismic section as a surface, which could be decomposed to orthogonal components (principal components) from its two-dimensional auto correlation function. Obviously, each orthogonal component is a surface where stacking these surfaces yields the original surface. Moreover, orthogonality here means that the correlation coefficient between any two components or surfaces is close to zero. Thus, calculation of principal components reduces

calculation of eigenvectors and eigenvalues of two-dimensional autocorrelation function of the original surface. Subsequently, descending sorting of principal components was performed by their contribution to the total variance (amplitude) of the studied surface. Matrix of eigenvectors and diagonal matrix of eigenvalues are related to each other by covariance matrix of multidimensional vector as follows [3]:

$$\Lambda = \varphi^T C \varphi \quad (1)$$

where C is the covariance matrix for the multidimensional vector. φ is the matrix of eigenvectors that are orthogonal to each other, and Λ is the diagonal matrix of eigenvalues. It should be noted that the eigenvectors corresponding to principal components are uncorrelated, which is the principle of orthogonality. The eigenvector that is corresponding to the maximum eigenvalue of the covariance matrix can determine the first principal component. Usually, for fault detection purposes on seismic data, the first principal component contains most of the relevant information of the studied seismic section. The other major components are related to local peculiarities of the seismic section and their linear combination can explain other properties of fault in seismic section. Obviously, random noise in seismic data will exhibit no correlation with fault properties in attributes and other latent features that results to suppression of noise in the final stacked image of principal components.

3. Application on the field land data

3.1. Geology of the study area

To investigate the efficiency of the proposed approach, the method was applied on a field seismic data from northeast of Iran. The study area is located in the eastern coast of the Caspian Sea, called the Gorgan plain (Fig. 1a). The region contains thick layers of sediments of Jurassic to Miocene age. The petrology of the sediment sequences in the region consists of shale, limestone, marl, sandstone, and partially conglomerates and evaporates (Fig. 1b). This sequence locates beneath an unconformity of Paleocene conglomerates. The aim of seismic investigation here was exploration of structures related to gas reservoirs. However, the area contains numerous mud volcanoes that some of them are related to gas reservoirs. It should be mentioned that young active mud volcanoes in the Gorgan plain are surficial. The old and inactive mud volcanoes, however, are in deeper parts, and they are believed to harden and dewater the shale unit with conical shape (called finger shape) like as mud volcanoes. Upcoming movement of mud also made an anticline shape in its upper sediments accompanied with normal faulting, which is a common phenomenon in such areas. Regardless of the nature of these finger-shape structures, enhancing seismic image of faults and boundary of these structures is the aim of applying the proposed approach on the dataset. The length of the seismic profile is 35 km with 465 explosive sources and 96 active receiver channels recorded the data. The minimum and maximum offsets were 140 meters and 3458 meters, respectively. The group interval was 35 meters and the source interval was set to 70 meters. Table 2 represents the profile geometry of the seismic acquisition.

Table 2. Acquisition parameters of the seismic line [30].

Geometry of mid-point and offset		Source and receiver geometry	
Number of CMP	1952	Source number	465
Fold	24	Source interval	70 m
CMP distance	17.5 m	Receiver number	997
Offset	140-3458	Receiver interval	35 m
Frequency parameters		**Recording parameters**	
Frequency content	100 -8 Hz	Record Time	7 S
Dominant frequency	20 Hz	Sampling interval	4 ms

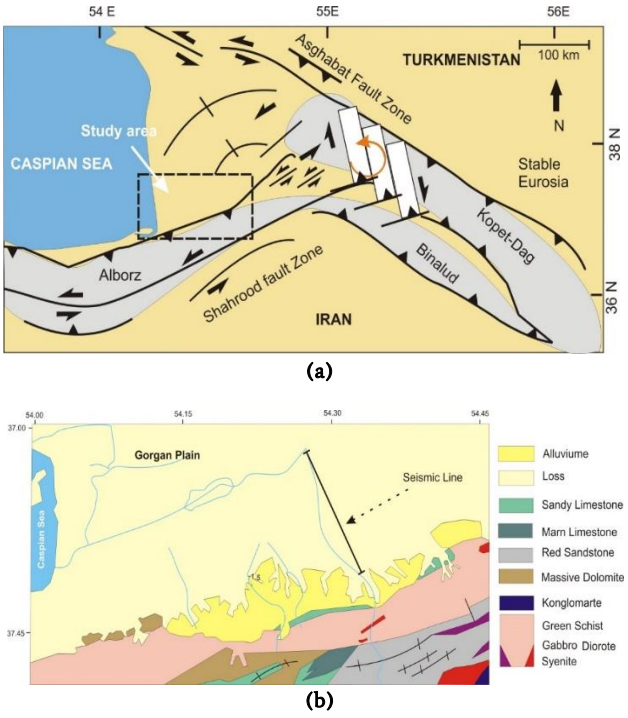

Fig. 1 (a). Location of the study area in SE of the Caspian Sea in the Gorgan Plain shown by dashed rectangle. **(b)** The geological map of the study area and the seismic profile shown by black line [29].

3.2. Fault detection by proposed PCA approach

Fig. 2 shows the seismic section of the study area. As it is seen, the seismic image shows high quality and high signal to noise ratio in the upper part, and represents lower quality with more random noise in larger depths. Sedimentary layers in top of the section show thickening and dipping to right. An unconformity from older sequence in larger depths separates these thick sediments. The unconformity shows dipping to right of the section, as well.

Three mud volcanoes resembling a finger shape are located beneath the unconformity and their effect on anticlinal shape of the upper sediments is obvious. All these geological objects were shown in seismic section of Fig. 2. The boundary of mud volcanoes and faults drawn in Fig. 2 are the result of primary interpretation on conventional seismic image. It is supposed that by applying the proposed method, more faults and accurate position and shape of the mud volcanoes could be imaged. Chaos seismic attributes is an interpretation tool that could differentiate various seismic pattern in seismic image. Based on the change of physical properties of the wave propagation media in subsurface, which is the result of change in lithology, seismic signals show different shape. This difference in seismic signal form is used to separate various lithologies or geological structures based on the seismic pattern. Usually, seismic signals in a sequence of sedimentary layers show high similarity from trace to trace, while in some geological objects the similarity is too low, such as salt dome or mud volcanoes, where no distinct reflector appears in that structure. Thus, the seismic pattern in latter examples shows a chaos and the former media shows a non-chaotic seismic pattern. The chaos attribute measures this similarity and separates chaotic pattern from non-chaotic seismic pattern in seismic image. Fig. 3a shows the result of seismic chaos attribute on seismic image. As it is seen in Fig. 3a, areas that were indicated as possible mud volcano bodies show chaotic pattern, while other part of seismic image show layered and non-chaotic pattern. Faulted area above the mud volcano also show chaotic pattern due to complexity of wave propagation in the media and low similarity between the seismic signal shapes from trace to trace near faults. Thus, although this area with chaotic pattern indicates faulting in layer, the resolution of this attribute is not high enough to trace the faults based on this attribute only. Two other major attributes that are

used for fault imaging are the first and second derivatives of the seismic signals. These attributes are the results of advances in conventional curvature attributes. These attributes were introduced as amplitude curvature (as opposed to the structural curvature), which involves the first and second derivatives of only the seismic data [21].

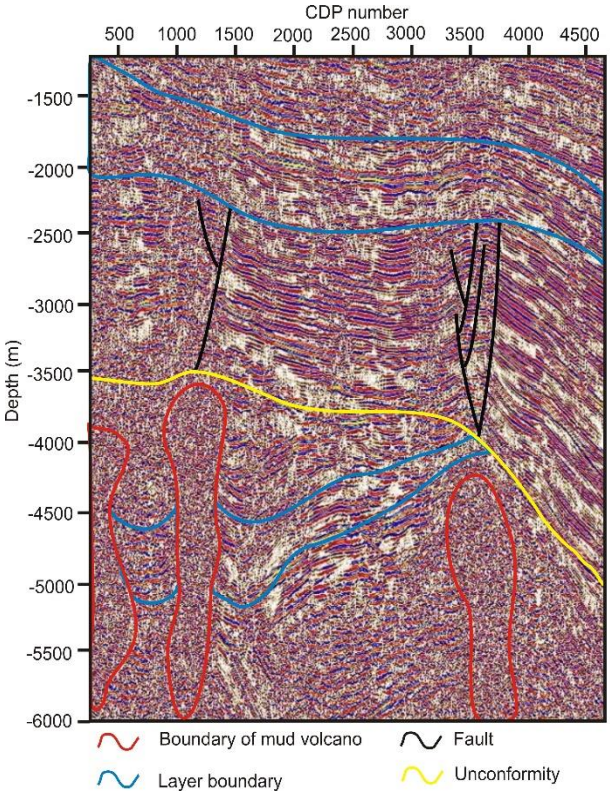

Fig. 2. The seismic image shows three possible mud volcanoes beneath an unconformity with listric normal faults.

$$\frac{\partial S}{\partial x},\ \frac{\partial S}{\partial y},\ \frac{\partial^2 S}{\partial x^2},\ \frac{\partial^2 S}{\partial y^2} \Rightarrow$$
$$a_{\psi} = \frac{\partial S}{\partial \psi} = Cos\psi \frac{\partial S}{\partial x} + Sin\psi \frac{\partial S}{\partial y},\quad e_{\min} = \tfrac{1}{2}\left(\frac{\partial^2 S}{\partial x^2} + \frac{\partial^2 S}{\partial y^2}\right) \tag{2}$$

where S shows the seismic signal, a_{ψ} denotes the amplitude curvature at an azimuth angle ψ, and e_{mean} is the mean amplitude curvature. Arbitrary direction of derivation also is shown by y and x. The first derivative usually identifies sharp interfaces and discontinuities in seismic image. It also indicates the changes in reflectivity and interprets as an index for absorption of energy in different layers. The second derivative is conventionally used to identify sharp changes in lithologies as an estimate for sharpness of seismic events. It can also be used to show all reflecting interfaces visible within seismic band-width. Therefore, it is supposed that these attributes are used to enhance faults and boundary of mud volcanoes in seismic images. Fig 3b and 3c show the first and second attributes derivatives of the seismic image, respectively. As it is seen on derivative attribute images (Figs. 3b and 3c), faults were clearly imaged by the first derivative attributes, while the second derivative can better image sharp changes in sedimentary sequences and separate body of mud volcanoes from dipping sedimentary layers. The variance attribute, which is usually known as the opposite of coherency, represents the trace-to-trace variability over a particular sample interval, and therefore, produces interpretable lateral changes in seismic image. Obviously, similar traces in seismic image produce low variance coefficients, while discontinuities remain with high coefficients. Since faults may cause discontinuities in the neighboring lithologies, and subsequently in the trace-to-trace variability, therefore, they become detectable by variance seismic attributes. Fig. 3d shows seismic attribute image of variance of the study data. The variance image can clearly enhance faults, while it is not able to define accurately the boundary of mud volcanoes. The four other attributes were related to curvature of the reflector. The curvature attribute can be estimated from a time structure map by fitting the local quadratic surface given by [25]:

$$t(x,y) = \left[ax^2 + by^2 + cxy\right] + \left[dx + ey + f\right] \tag{3}$$

where a, b and c are constant parameters related to dip of the structures in x and y direction related to an ellipsoid, while d and e are linear dips in x and y direction show a dipping plane. The parameter f is also a constant parameter related to a dipping plane that shows an estimation of the plane location. These parameters are fined by fitting a surface on seismic data. When a, b and c are zero, the structure shows only a dipping plane indicating the fault surface. For a curved surface, the following curvature attributes called minimum curvature K_{min} and maximum curvature, K_{max} could be extracted by [25]:

$$K_{\max} = K_{mean} + \sqrt{K_{mean}^2 - K_{gauss}},\quad K_{\min} = K_{mean} - \sqrt{K_{mean}^2 - K_{gauss}},$$
$$K_{gauss} = \frac{4ab - c^2}{\sqrt{1 + d^2 + e^2}},\quad K_{mean} = \frac{a(1+e^2) + b(1+d^2) - cde}{\sqrt[3]{1 + d^2 + e^2}} \tag{4}$$

By combination of these curvature attributes, two other curvatures called the most positive curvature, K+, and the most negative curvature, K-, are extracted as follow [25]:

$$K_{+} = (a+b) + \sqrt{(a-b)^2 - c^2},\quad K_{-} = (a+b) - \sqrt{(a-b)^2 - c^2} \tag{5}$$

Due to the large number of attributes images, these four attribute sections were not shown here, however, they were used to calculate the covariance matrix and contributed in attribute stacking procedure.

Subsequently, the eight seismic attributes were used to detect faults in this image for the PCA procedure. It should be noted that prior to the PCA procedure on these eight attributes, it is required to perform a normalization step. Table 3 shows the result of PCA of seismic attributes with the percentages of variance for each attribute. According to the coefficients in Table 3, equations of the principal component were provided to present the variance.

According to the coefficients in Table 3, only the first four components contain required relevant information for fault image enhancement, whose equations are:

$$PC1 = 0.000115(chaos) + 0.000504(D1) - 0.000120(D2) + 0.000596(Var) + 0.707903(k\max) + 0.706309(K\min) - 0.000760(k+) - 0.000747(k-) \tag{6a}$$

$$PC2 = 0.00045(chaos) + 0.000567(D1) + 0.000389(D2) + 0.000296(Var) + 0.706309(k\max) + 0.707903(K\min) - 0.000208(k+) + 0.000027(k-) \tag{6b}$$

$$PC3 = 0.173627(chaos) - 0.12866(D1) + 0.2656(D2) + 12816(Var) + 0.000430(k\max) - 0.000823(K\min) + 0.3859(k+) + 0.84699(k-) \tag{6c}$$

$$PC4 = 0.12964(chaos) - 0.2428(D1) + 0.06075(D2) + 0.01927(Var) - 0.000087(k\max) - 0.000394(K\min) + 0.8626(k+) + 0.4194(k-) \tag{6d}$$

By stacking the information of components in each image related to equations (6a-d), the stacked images of the attributes could be extracted which could be used for primary structural interpretation. Fig. 4 shows a stacked image of the seismic data obtained from stacking the related attributes. As it is seen on the stacked image of Fig. 4, random noise was dramatically reduced in the final image. Not only the targets of imaging, being faults and mud volcano bodies, but also other geological structures such as layer boundaries and unconformity were also enhanced due to reduction of noise and stacking coherent signals. Primary interpretation of structures on Fig. 4 shows better and more accurate location of faults and mud volcano bodies compared to Fig. 2.

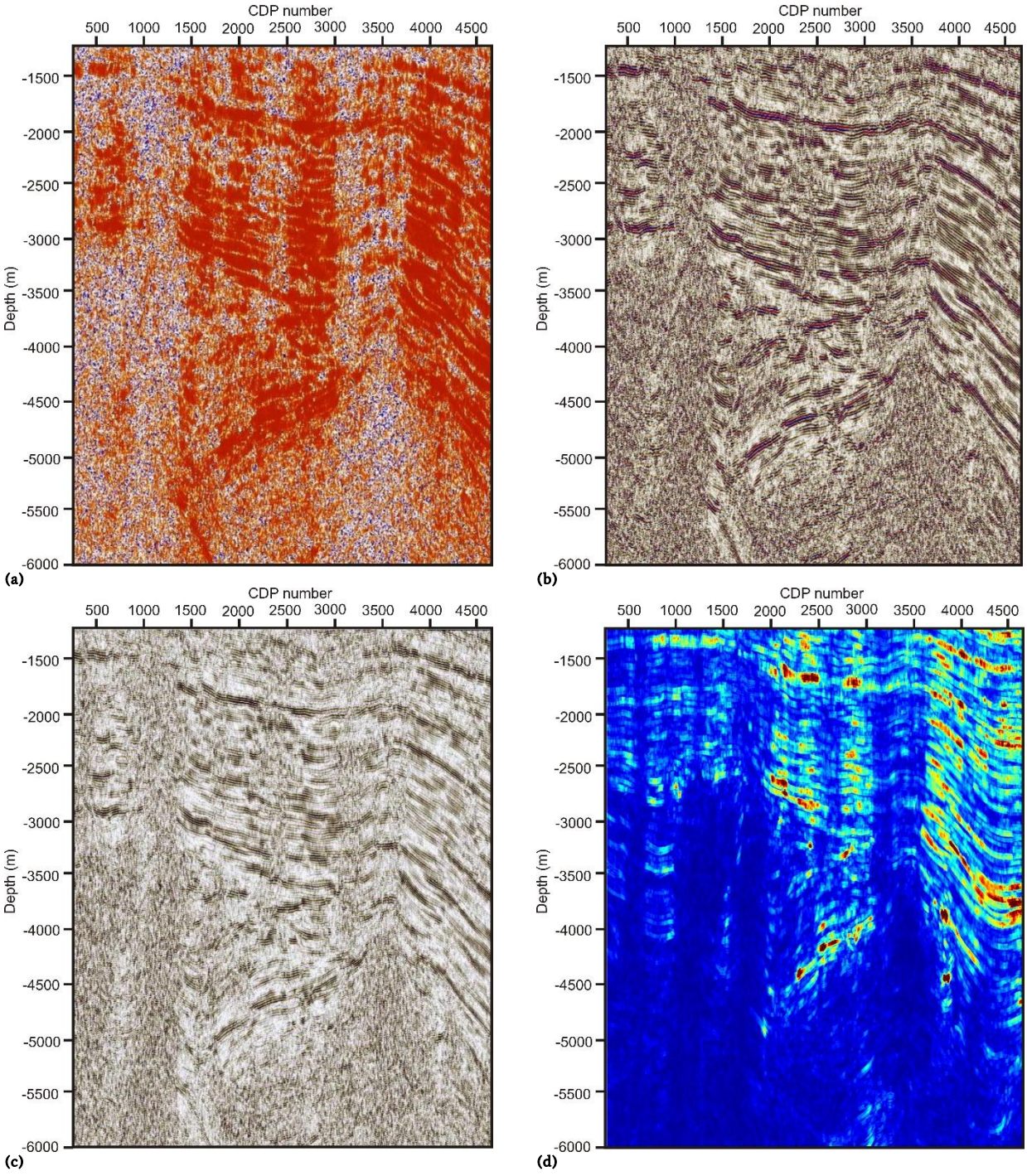

Fig. 3. Illustrations of (a) the chaos, (b) the first derivative, (c) the second derivative and (d) the attributes variance on the seismic image.

3.3. The RGB representation

The RGB representation is an interpretation tool in image processing literature that brings the information of three components in one image by false color composition of three images. The RGB colored image is an additive color model in which red, green and blue colors are added together in various ways to reproduce a broad array of colors. It is called false color composite (FCC), since it is a composition procedure of three images that are not represented by their true colors and the dedicated colors to each picture are false colors. In the procedure of creating the RGB image from principal components, the operator allocates each color, (red, green and blue) to each component image. Subsequently, the RGB image is illustrated by pixel by pixel mathematical stacking of each component. The result is a colored image that has a broad band of colors regarding the percentage of variance obtained in PCA for each image. The color of each pixel also depends on which color is dedicated to which components and which three components are added together by which sequence. Therefore, based on the target of interpretation, various number of RGB illustration can be obtained from several of components. To have a section of enhanced imaging of fault, the first four principal components images produced by equation 6a-d were selected for FCC procedure to produce a final RGB image. These four components image are shown in Figs. 5a-d. To create an RGB image with four components, 24 different composition states are possible based on

which color is allocated to which component. It depends on the interpreter's choice and the analysis that which color composition would yield the highest contrast between the target of study in image and the rest of the image.

Table 3. Principal components analysis of eight seismic attributes.

Principal Component	Chaos attribute	First derivative attribute (D1)	Second derivative attribute (D2)	Variance attribute (var)	Maximum curvature attribute (k max)	minimum curvature attribute (k min)	Most maximum curvature attribute (k+)	Most minimum curvature attribute (k-)	Percent of variance
PC1	0.00012	0.0005	-0.0001	0.000596	0.7079	0.7063	-.00076	-0.00075	29.12
PC2	0.00005	0.0006	0.0004	0.000296	0.7063	0.7079	-0.0002	0.00003	27.47
PC3	0.17363	-0.1287	0.2656	0.128161	0.0004	-0.0008	0.3859	0.84699	20.80
PC4	0.12964	-0.2428	0.0608	0.019273	-0.0001	-0.0004	0.8627	0.41949	19.06
PC5	-0.10947	-0.0739	-0.3035	-0.925642	-0.00006	0.0005	0.0772	-0.01664	1.04
PC6	-0.02845	-0.5655	-0.7230	-0.243177	-0.00090	0.0003	-0.2869	-0.13844	1.03
PC7	0.06165	-0.7712	-0.5608	0.244115	0.00032	0.00004	0.1348	-0.09582	0.98
PC8	-0.96771	-0.0668	0.0197	-0.087535	-0.00025	0.00009	0.0206	-0.22495	0.50

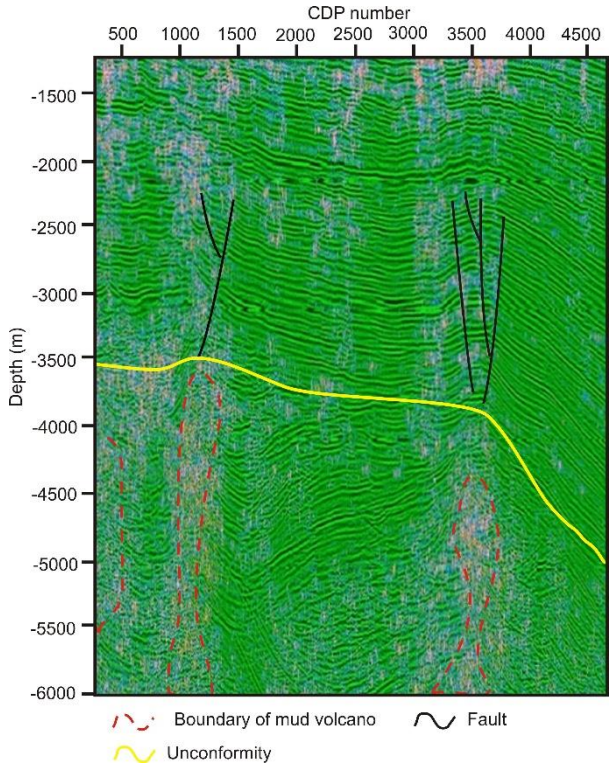

Fig. 4. illustration of stacking the fault enhancement related attributes according to PCA of eight analyzed attributes according to Table 3.

According to the analysis that was performed on this study, the composition of FCC by PC1, PC2 and PC4 for red, green and blue, respectively, (easily could be written FCC-124), FCC-134 and FCC-234 obtained the image with the highest enhancement on fault and boundary of mud volcanoes in the image with the highest quality. The RGB illustrations are shown in Figs. 6-8.

Fig. 6 shows the RGB image obtained by FCC-124. As shown in the RGB image of Fig. 6, the faults were enhanced in comparison to conventional image. The yellow line on Fig. 6 shows the unconformity and the black lines show listric normal faults above the unconformity in the top of each mud volcano. Red lines also show the boundary of mud volcanoes that can be traced accurately in this FCC. A sample of layer boundary also were illustrated in this image by blue line that shows the ability of this approach in enhancing fault and sedimentary layer sequence boundary altogether.

Fig. 7 shows the RGB image obtained by FCC-134. Based on the interpretation analysis of Fig. 7, this FCC is less sensitive to noise and can better enhance the fault position and the objects boundary compared to Fig. 6. Thus, it is supposed that more faults are imaged and the boundary of mud volcanoes might change. By more interpretation on Fig. 7, some faults were imaged in the left part of the section and the boundary of mud volcanoes in the center of the section was changed, as well. This image shows that the mud volcano has a narrower body compared to Fig. 6. Interpreter's analysis determines the correct interpretation. However, the final evaluation of the interpretation model would be performed by borehole drilling data, which is not available in this study.

Fig. 8 shows the RGB image obtained by FCC-234. This composition of colors would yield the image with the most enhanced fault. Thus, it is supposed that more faults can be traced in Fig. 8. Black line on Fig. 8 shows the location of faults, which illustrates more faults on the section. However, since this FCC is adopted for fault enhancement, it cannot define accurate boundary of mud volcanoes. Therefore, in Fig. 8, the mud volcanoes were shown by dashed line, which depicts more uncertainty compared to Figs. 6 and 7, i.e. only for mud volcanoes boundary, while more faults were better enhanced. Finally, based on the interpretation target, the interpreter could make a trade-off between different RGB images obtained by various FCC or could build a hybrid geological model by integration of different results.

4. Conclusion

Enhancing faults and geological structures boundary is a controversial task in seismic image interpretation. There are various approaches to extract as much as possible relevant information for fault and reflector truncation imaging from seismic data. Seismic attributes are in extensive use for this task. However, there are also various types of data integration approaches to combine information from seismic attributes. The approach introduced here was to combine seismic attributes by PCA analysis. The PCA analysis used here showed that four seismic attributes, considering chaos, the first and second derivatives and variance, have the most relevant information for fault and geological object boundary enhancement in seismic imaging. Afterwards, stacking these images showed that not only random noises from data are reduced, but also the quality of seismic image is improved

and the faults were enhanced in final stacked seismic image. Primary interpretation on attribute-stacked image showed that this image is more appropriate for interpretation than the seismic one. Creating the matrix of covariance also showed the percentage of information that could be extracted from each image. Subsequently, an RGB representation of the first four PCA could also enhance more faults and geological structures boundary. The RGB illustrations were created by various integrations approaches of PCA images by false color composition of attributes. Here, we used PCA by deriving the equations that show the percentage of contribution of each attribute in a principal component image. Three RGB images were created by composing attributes by FCC-124, FCC-134 and FCC-234. Interpretation on FCC-124 showed that it would be an appropriate image for imaging unconformity, faults and mud volcano bodies. However, the FCC-134 could better enhance faults, while it shortens the width of geological structures. Afterwards, the FCC-234 revealed that this composition could better enhance faults than the other two FCC images. However, this composition failed to image the truncation of reflectors with mud volcano bodies. Thus, it would be a trade-off for interpreter to select which FCC image suits the target of interpretation. Results have shown that FCC-234 is appropriate for fault enhancement and FCC-134 can be used for imaging the boundary of geological objects. In this step, only the interpretation tools and the interpreter's knowledge can evaluate these images. However, the final evaluation of these models can only be performed by the data obtained from borehole drilling, which is not available in most of seismic studies. Thus, it is necessary to perform an uncertainty analysis on models to define the uncertainty of each model and define the exact location of drilling targets.

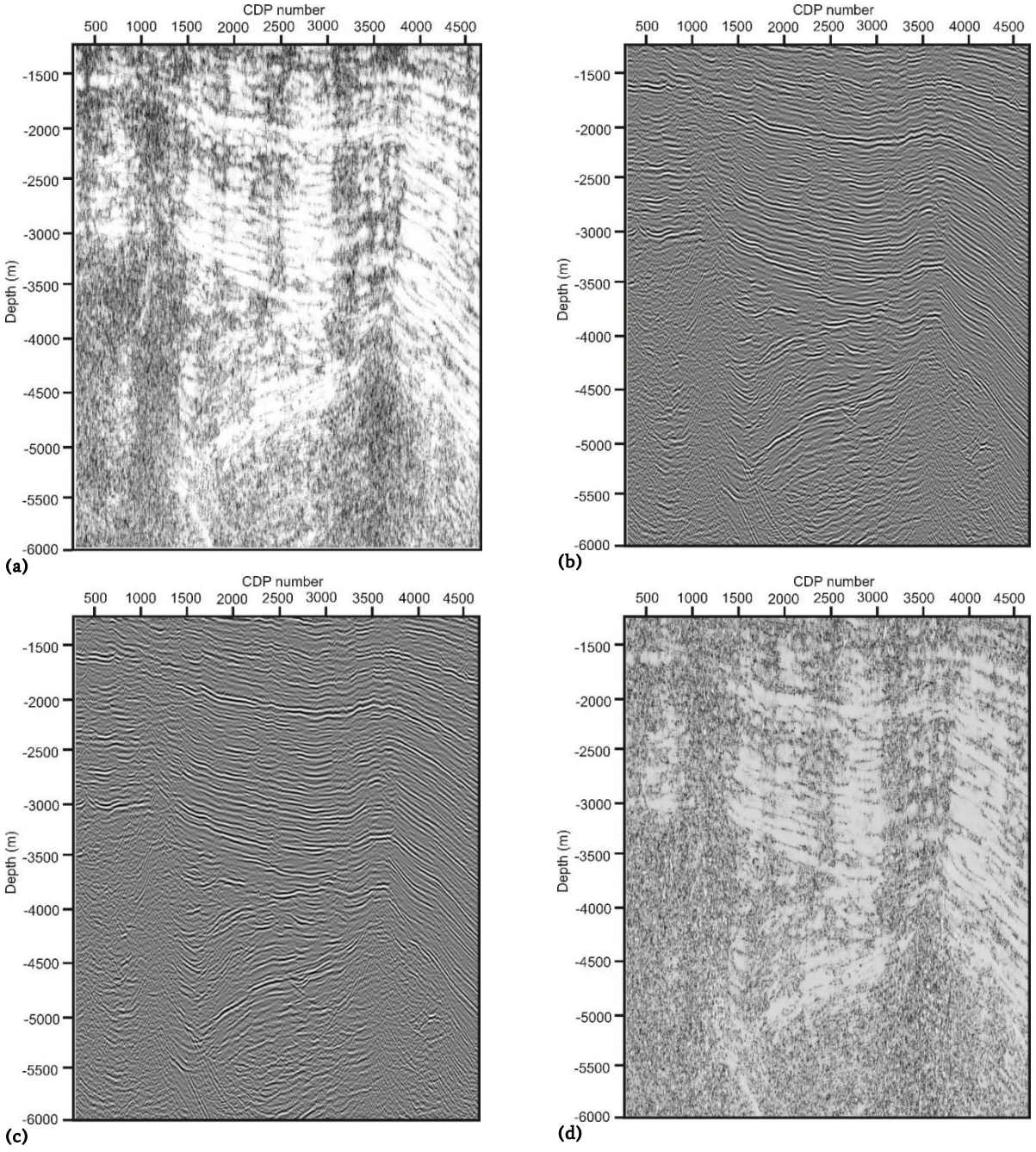

Fig. 5. Principal component illustration of images obtained by (a) equation (6a), (b) equation (6b), (c) by equation (6c) and (d) by equation (6d).

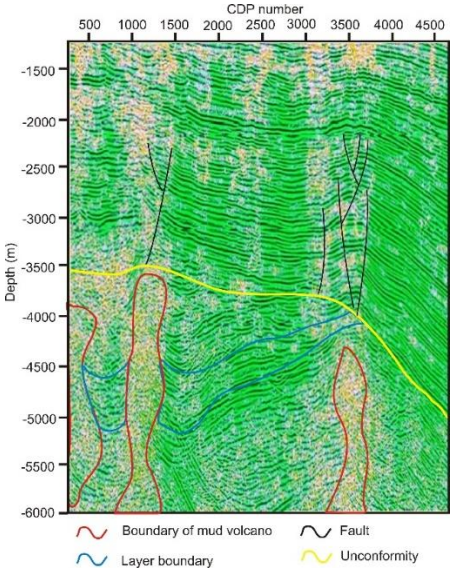

Fig. 6. Color Composite of the seismic image: Red: PC1; Green: PC2; Blue: PC4.

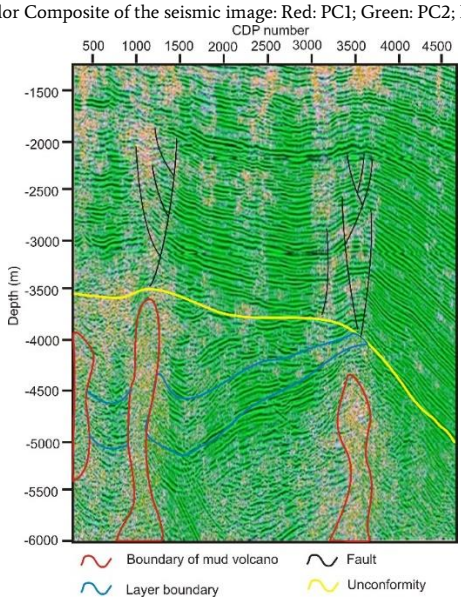

Fig. 7. Color Composite of the seismic image: Red: PC1; Green: PC3; Blue: PC4.

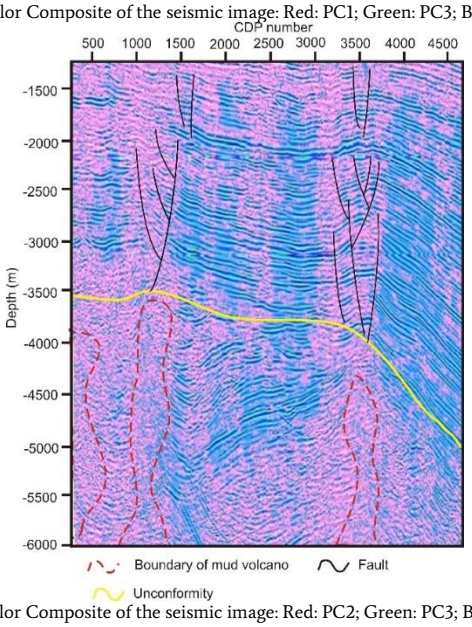

Fig. 8. Color Composite of the seismic image: Red: PC2; Green: PC3; Blue: PC4.

References

[1] Mohammad-Abadi, H., Edalat, A., & Siahkoohi, H., (2012). Applying horizon-based attributes to detect faults/fractures, Journal of the Earth and Space Physics, 3, 73-84.

[2] Daly, R.M., Gevers, E.C.A., Stampfli, G.M., Davies, D.J., Gastaldi, C.N., Rujitenberg, P.A., & Vermer, G.J.O., (1989). Dip and azimuth display for3-D seismic interpretation, First break, 7 (3), 86-95, https://doi.org/10.3997/1365-2397.2007031

[3] Priezzhev, L.L. & Scollard, A. (2012). Faults and fracture Detection based on seismic surface Orthogonal Decomposition, EAGE Conference & Exhibition incorporating SPE EUROPEC, Copenhagen, Denmark, 4-7 Jume,74.

[4] Scheevel, J.R. & Payrazyan, K. (1999). Principal component analysis applied to 3D seismic data for reservoirs property estimation, SPE Annual Technical Conference and Exhibition, Houston, Texas, 3-6 October.

[5] Jeong , W., Whitaker, R., & Dobin, M., (2006). Interactive 3D seismic fault detection on the Graphics Hardware, Volume Graphics, 24, 111-118, https://doi.org/10.2312/VG/VG06/111-118

[6] Jaglan. H., Qayyum, F., & Huck, H. (2015). Unconventional seismic attributes for fracture characterization, First Break, 33, 101-109.

[7] Mirkamali, M.S., Ramazi, H.R., Bakhtiari, M.R., & Ramesh, H. (2015). Compilation of seismic attributes and artificial neural networks in identifying faults systems in the Hormuz strait area., Geosciences, 24, 351-358.

[8] Tingdahl, K., & Hemstra, N. (2003). Estimating fault-attribute orientation with gradient analysis, Principle component analysis and localized Hough-transform, 37th Annual International Meeting, SEG, Expanded Abstract, 358-361.

[9] Guo, H. K., K. J. Marfurt, & J. Liu, (2009), Principal component spectral analysis: Geophysics, 74(4),P35–P43, http://dx.doi.org/10.1190/1.3119264

[10] Chopra, S., & Marfurt, K. (2014). Churning seismic attributes with principal component analysis, SEG Technical Program Expanded Abstract, 2672-2676. https://doi.org/10.1190/segam 2014-0235.1

[11] Kirkham, C., Cartwright, J., Hermanrud, & C., Jebsen, C., (2017). The spatial, temporal and volumetric analysis of a large mud volcano province within the Eastern Mediterranean. Marine and Petroleum Geology, 81, 1-16. http://dx.doi.org/10.1016/j.marpetgeo.2016.12.026

[12] Dimitrov, L.I., (2002), Mud volcanoes—the most important pathway for degassing deeply buried sediments. Earth-Science Reviews 59, 49–76. https://doi.org/10.1016/S0012-8252(02)00069-7

[13] Fowler, S., Mildenhall, J., Zalova, S., Riley, G., Elsley, G., Desplanques, A., & Guliyev, F., (2000). Mud volcanoes and structural development on Shah Deniz. Journal of Petroleum Science and Engineering. 28, 189-206. https://doi.org/10.1016/S0920-4105(00)00078-4

[14] Qi, J., Lin, T., Zhao, T., Li, F, & Marfurt, K., (2016), Semisupervised multiattribute seismic facies analysis. Interpretation, 4(1), SB91-SB106, https://doi.org/10.1190/INT-2015-0098.1

[15] Pussak, M., Bauer, K., Stiller, M., & Bujakowski, W., (2014), Improved 3D seismic attribute mapping by CRS stacking instead of NMO stacking: Application to a geothermal reservoir in the Polish Basin, Journal of Applied Geophysics. 103, 186-198, https://doi.org/10.1016/j.jappgeo.2014.01.020

[16] Somoza, L., Medialdea, T., León, R., Ercilla, G., Vázquez, J.T., Farran, M., Molina, J.H., González, J., Juan, C., & Puga, M.C.F., (2012). Structure of mud volcano systems and pockmarks in the region of the Ceuta Contourite Depositional System (Western Alborán Sea). Marine Geology, 332, 4–26, http://dx.doi.org/10.1016/j.margeo.2012.06.002

[17] Amin, A., Deriche, M., Shafiq, M.A., Wang, Z., & AlRegib, G., (2017).

Automated salt-dome detection using an attribute ranking framework with a dictionary-based classifier. Interpretation, 5(3), SJ61-SJ79. https://doi.org/10.1190/INT-2016-0084.1

[18] Bourget, J., Ainsworth, R.B., & Thompson, S., (2014). Seismic stratigraphy and geomorphology of a tide or wave dominated shelf-edge delta (NW Australia): Process-based classification from 3D seismic attributes and implications for the prediction of deep-water sands. Marine and Petroleum Geology, 57, 359-384. http://dx.doi.org/10.1016/j.marpetgeo.2014.05.021

[19] Moss, J., Cartwright, J., Cartwright, A., & Moore, R., (2012). The spatial pattern and drainage cell characteristics of a pockmark field, Nile Deep Sea Fan. Marine and Petroleum Geology. 35, 321-336. https://doi.org/10.1016/j.marpetgeo.2012.02.019

[20] Bitrus, P.F., Iacopini, D., & Bond, C.E., (2016). Defining the 3D geometry of thin shale units in the Sleipner reservoir using seismic attributes. Marine and Petroleum Geology, 78,405-425, https://doi.org/10.1016/j.marpetgeo.2016.09.020

[21] Chen, S.C., Hsu, S.H., Wang, Y., Chung, S.H., Chen, P.C., Tsai, C.H., Liu, C.S., Lin, H.S., & Lee, Y.W., (2014). Distribution and characters of the mud diapirs and mud volcanoes off southwest Taiwan. Journal of Asian Earth Sciences. 92, 201-214, https://doi.org/10.1016/j.jseaes.2013.10.009

[22] Aqrawi, A.A., Weinzierl, W., Daber, R., & Boe, T.H., (2012). Directional guided seismic attributes and their use in assisting structural, stratigraphic and lithological interpretation. 82nd SEG annual meeting, https://doi.org/10.1190/segam2012-0674.1

[23] Raef, A.E., Meek, T.N., & Totten, M.W., (2016), Applications of 3D seismic attribute analysis in hydrocarbon prospect identification and evaluation: Verification and validation based on fluvial palaeochannel cross-sectional geometry and sinuosity, Ness County, Kansas, USA. Marine and Petroleum Geology, 73, 21-35, http://dx.doi.org/10.1016/j.marpetgeo.2016.02.023

[24] Lykousis, V., Alexandri, S., Woodside, J., de Lange, G., Da¨hlmann, A., Perissoratis, C., Heeschen, K., Ioakim, C., Sakellariou, D., Nomikou, P., Rousakis, G., Casas, D., Ballas, D., & Ercilla, G., (2009). Mud volcanoes and gas hydrates in the Anaximander mountains (Eastern Mediterranean Sea). Marine and Petroleum Geology, 26, 854–872, https://doi.org/10.1016/j.marpetgeo.2008.05.002

[25] Berthelot, A., Solberg, A.H.S., & Gelius, L.J. (2013). Texture attributes for detection of salt. Journal of Applied Geophysics, 88, 52–69, http://dx.doi.org/10.1016/j.jappgeo.2012.09.006

[26] Farfour, M., Yoon, W.J., & Kim, J., (2015). Seismic attributes and acoustic impedance inversion in interpretation of complex hydrocarbon reservoirs. Journal of Applied Geophysics 114, 68–80, http://dx.doi.org/10.1016/j.jappgeo.2015.01.008

[27] Miller, P., Dasgupta, S., & Shelander, D., (2012). Seismic imaging of migration pathways by advanced attribute analysis, Alaminos Canyon 21, Gulf of Mexico. Marine and Petroleum Geology, 34, 111-118, http://dx.doi.org/10.1016/j.marpetgeo.2011.09.005

[28] Baghzendani, H.R., Aghajani, H. & Solimani, M. (2015). Subsurface modeling of mud volcanoes, using density model and analysis of seismic velocity. Journal of Mining & Environment, 6 (1), 31-39.

[29] Hollingsworth, J., Jackson, J., Walker, R., Gheitanchi, M.R., & Boloutchi, M.J. (2006). Strike-Slip faulting, rotation and along-strike elongation in the Kopeh Dagh Mountains, NE Iran. Geophysical Journal International, 166, 1161-1177. https://doi.org/10.1111/j.1365246X. 2006 .02983.x

[30] Baghzendani, H.R. (2014), Master Thesis, “Detection mud volcanoes with using of joint Interpretation gravity and seismic method”, Shahrood university of technology.